Redox Biology 36 (2020) 101610

Contents lists available at ScienceDirect

Redox Biology

journal homepage: www.elsevier.com/locate/redox

Research Paper

Nanoformulation of the superoxide dismutase mimic, MnTnBuOE-2-PyP^{5+}, prevents its acute hypotensive response

Sarah L. Schlichte [a], Svetlana Romanova [b], Kenichi Katsurada [a], Elizabeth A. Kosmacek [c], Tatiana K. Bronich [b], Kaushik P. Patel [a], Rebecca E. Oberley-Deegan [c], Matthew C. Zimmerman [a,*]

[a] Department of Cellular and Integrative Physiology, University of Nebraska Medical Center, Omaha, NE, United States
[b] Department of Pharmaceutical Sciences and Center for Drug Delivery and Nanomedicine, University of Nebraska Medical Center, Omaha, NE, United States
[c] Department of Biochemistry and Molecular Biology, University of Nebraska Medical Center, Omaha, NE, United States

ARTICLE INFO

Keywords:
MnTnBuOE-2-PyP^{5+}
Mesoporous silica nanoparticle
SOD Mimic
Blood pressure
Renal sympathetic nerve activity

ABSTRACT

Scavenging superoxide ($O_2^{\bullet-}$) via overexpression of superoxide dismutase (SOD) or administration of SOD mimics improves outcomes in multiple experimental models of human disease including cardiovascular disease, neurodegeneration, and cancer. While few SOD mimics have transitioned to clinical trials, MnTnBuOE-2-PyP^{5+} (BuOE), a manganese porphyrin SOD mimic, is currently in clinical trials as a radioprotector for cancer patients; thus, providing hope for the use of SOD mimics in the clinical setting. However, BuOE transiently alters cardiovascular function including a significant and precipitous decrease in blood pressure. To limit BuOE's acute hypotensive action, we developed a mesoporous silica nanoparticle and lipid bilayer nanoformulation of BuOE (nanoBuOE) that allows for slow and sustained release of the drug. Herein, we tested the hypothesis that unlike native BuOE, nanoBuOE does not induce an acute hypotensive response, as the nanoformulation prevents BuOE from scavenging $O_2^{\bullet-}$ while the drug is still encapsulated in the formulation. We report that intact nanoBuOE does not effectively scavenge $O_2^{\bullet-}$, whereas BuOE released from the nanoformulation does retain SOD-like activity. Further, in mice, native BuOE, but not nanoBuOE, rapidly, acutely, and significantly decreases blood pressure, as measured by radiotelemetry. To begin exploring the physiological mechanism by which native BuOE acutely decreases blood pressure, we recorded renal sympathetic nerve activity (RSNA) in rats. RSNA significantly decreased immediately following intravenous injection of BuOE, but not nanoBuOE. These data indicate that nanoformulation of BuOE, a SOD mimic currently in clinical trials in cancer patients, prevents BuOE's negative side effects on blood pressure homeostasis.

1. Introduction

Superoxide ($O_2^{\bullet-}$) is one of the major reactive oxygen species (ROS) known to play a role in a wide variety of pathological conditions including various types of cancer, diabetes, hypertension and numerous other cardiovascular-related diseases [1,2]. As such, over the past several decades, numerous compounds have been developed to mimic superoxide dismutases (SOD), a group of endogenous enzymes responsible for scavenging $O_2^{\bullet-}$. Some of the most powerful SOD mimics are the manganese porphyrins, such as MnTE-2-PyP^{5+} (T2E) and MnTnBuOE-2-PyP^{5+} (BuOE) [2,3].

Numerous *in vivo* experimental studies have demonstrated therapeutic effects of SOD mimics. In particular, SOD mimics have been shown to be beneficial in various rodent models of cancer as radioprotectors. That is, during radiation, SOD mimics have been shown to prevent normal tissue injury while simultaneously suppressing tumor growth [2]. In a prostate cancer radiation model, Oberley-Deegan's group has shown the radioprotective effects of T2E and BuOE to protect normal prostate tissue while inhibiting prostate cancer tumor growth [4]. In the same model, they have also shown the protective effects of T2E in reducing fibrosis of the bladder and skin of the lower pelvic region [5]. Studies by Weitzel et al. have shown long-term radioprotective effects of BuOE in the brain four months after a single radiation treatment [6,7]. Numerous other studies have shown similar radioprotective

* Corresponding author. Department of Cellular and Integrative Physiology, Free Radicals in Medicine Program, University of Nebraska Medical Center, 985850 Nebraska Medical Center, Omaha, NE, 68198, United States.
E-mail address: mczimmerman@unmc.edu (M.C. Zimmerman).

https://doi.org/10.1016/j.redox.2020.101610
Received 1 May 2020; Received in revised form 1 June 2020; Accepted 15 June 2020
Available online 20 June 2020

effects of T2E and BuOE on salivary glands and mouth mucous [8–10], bone marrow [11], and the lungs [12,13].

These radioprotective therapeutic benefits have contributed to the clinical development of SOD mimics, particularly BuOE, due to its increase lipophilicity and reduced toxicity over T2E [14]. Currently, there are four on-going clinical trials utilizing BuOE (known as BMX-001) as a radioprotector (ClinicalTrials.gov Identifiers: NCT02655601, NCT02990468, NCT03386500, NCT03608020) [15]. However, previous non-clinical safety and toxicity studies have demonstrated that BuOE transiently alters cardiovascular function, including an increase in heart rate in non-human primates [16] and a significant decrease in blood pressure in dogs [16]. In an attempt to attenuate BuOE's acute hypotensive action, we developed a nanoformulation of BuOE (nanoBuOE) consisting of mesoporous silica nanoparticles and a lipid bilayer (Fig. 1). Mesoporous silica nanoparticles have been extensively used as drug carriers [17,18]. High surface area and large pore volume make them a perfect candidate for BuOE loading. This nanoformulation was also selected based on its potential for sustained delivery as well as its unique properties of controlled particle size and good biocompatibility. Herein, we tested the hypothesis that nanoBuOE fails to induce the acute hypotensive response observed by native BuOE because of the slow release properties of the nanoformulation. We report that nanoBuOE protects against the immediate, transient decrease in blood pressure and inhibition of sympathetic nerve activity that is characteristic of native BuOE.

2. Materials and methods

2.1. Materials

All reagents were used without further purification unless otherwise noted. Cetyltrimethylammonium bromide (CTAB) was purchased from MP Biomedicals (Solon, OH). Triethanolamine (TEAO) was purchased from ACROS Organics (Fair Lawn, NJ). Tetraethyl orthosilicate (TEOS), hypoxanthine (HX), xanthine oxidase (XO), bovine SOD protein, hydrogen peroxide (H_2O_2), acetylaminophenol (AAP), horseradish peroxidase (HRP), dietylenetriaminepentaacetic acid (DTPA), and bovine catalase protein were purchased from Sigma Aldrich (St. Louis, MO). 1-hydroxy-3-methoxycarbonyl-2,2,5,5-tetramethylpyrrolidine (CMH), diethyldithiocarbamic acid (DETC), and deferoxamine (DF) were purchased from Noxygen (Germany). BuOE was a kind gift from Dr. James Crapo, National Jewish Health, Denver, CO.

2.2. Native BuOE preparation

The powdered drug was kept at room temperature, under a vacuum seal, and away from water and light. At time of experimentation, the drug was weighed out and reconstituted in sterile PBS. The molarity of the solution was determined by spectrophotometer prior to sterilizing the drug with a syringe filter.

2.3. Synthesis of nanoBuOE

Mesoporous silica nanoparticles were prepared by the modified Stöber process via hydrolysis and condensation reaction of TEOS in the presence of CTAB surfactant as a micelle-forming (templating) agent. Lipid-coated mesoporous silica nanoparticles were synthesized as previously described [19–21]. In brief, the surfactant template, CTAB (0.25 g), was dissolved in distilled water (50 mL) and heated to 80 °C for 30 min while stirring. TEAO (80 μL) was added to the CTAB solution to pH ~9–9.5. Ethanol (EtOH, 1 mL) and the silicate source, TEOS (286 μL), were added drop-wise, and the reaction mixture was stirred for 1 h to allow for silica particle formation.

The size of the formed particles was about 40 nm as determined by dynamic light scattering (DLS). The silica colloidal dispersion was then disrupted with an equal volume of EtOH and centrifuged at 3500 rpm for 5 min. The collected pellet was washed by a mixture of EtOH and hydrochloric acid (HCl) (9:1, v/v) and stirred overnight at room temperature. After centrifugation (3500 rpm; 5 min), the obtained pellet was dissolved in EtOH (10 mL) and refluxed for 1–2 h to remove entrapped surfactant. After final centrifugation (10,000 rpm; 20 min), the pellet was dried under nitrogen at 40 °C for at least 4 h.

BuOE was loaded by rehydrating silica nanoparticles in aqueous solution of BuOE (feeding ratio 20% wt.) overnight upon mild agitation. After rehydration, the solution was centrifuged at 10,000 rpm for 30 min. Concentration of non-encapsulated BuOE in the supernatant was determined by measuring absorbance at 455 nm. The pellet containing BuOE-loaded silica was reconstituted with 1 mL of water and immediately added into a round bottom flask coated with dried lipid film. The lipid film was prepared by evaporation of a mixture containing distearoyl-*sn*-glycero-3-phosphocholine (DSPC), cholesterol, and 1,2-distearoyl-sn-glycero-3-phosphoethanolamine-N-[methoxy(polyethylene glycol)-2000] (DSPE-PEG_{2000}) at a molar percent ratio of 77.5:20:2.5 in chloroform and methanol (9:1, v/v), as previously described [20,21]. Following addition of BuOE-loaded silica particle suspension to the lipid dry film (1.1 wt equivalent of silica compare to lipid amount), the mixture was stirred for 1 h at 40 °C followed by probe sonication at 30 W for 10 min with 5–10 s on-off cycling. The particle size of BuOE-loaded

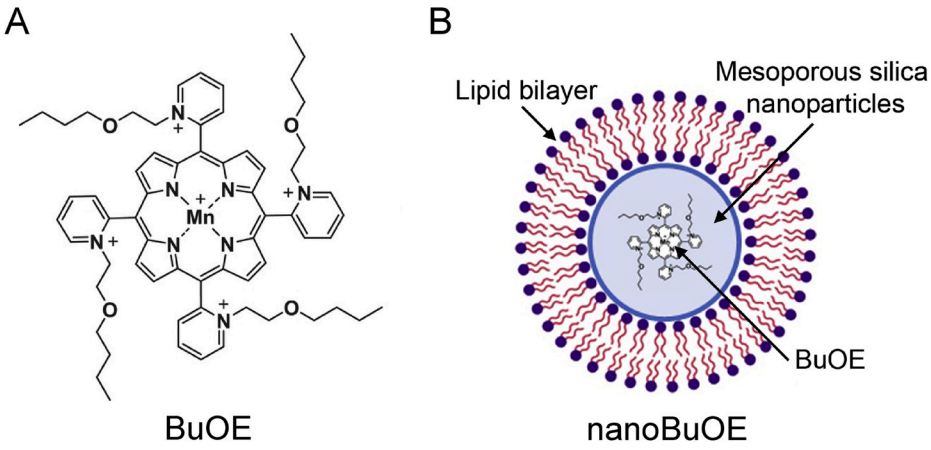

Fig. 1. Structure of MnTnBuOE-2-PyP^{5+} and its nanoformulation, nanoBuOE. A) Structure of MnTnBuOE-2-PyP^{5+} (BuOE). B) Structure of nanoBuOE. BuOE is encapsulated in mesoporous silica nanoparticles (blue) and wrapped in a lipid bilayer (purple and orange). (For interpretation of the references to colour in this figure legend, the reader is referred to the Web version of this article.)

coated silica nanoparticles was about 55 nm as determined by DLS. The drug encapsulation efficacy was found to be ca. 15% w/w.

2.4. Physicochemical characterization of silica nanoparticles

Hydrodynamic diameter of silica nanoparticles was determined by DLS using a ZEN3600 Zetasizer Nano-ZS (Malvern Instruments Ltd., MA, United States). All measurements were performed in triplicate at 25 °C. The physicochemical characteristics of the empty and BuOE-loaded mesoporous silica nanoparticles are reported in Table 1. Of note, shielding of the negatively charged silanol groups of the mesoporous silica nanoparticles was observed after surface coating with a lipid bilayer, resulting in BuOE-loaded nanoparticles that were essentially neutral by charge.

2.5. NanoBuOE release studies

The *in vitro* drug release profiles of nanoBuOE were recorded in PBS (pH 7.4) using the dialysis method [22]. NanoBuOE (1 mL, 0.25 mg/mL BuOE) was placed into a dialysis tube with a molecular weight cut-off (MWCO) of 3.5 kDa and dialyzed against 20 mL PBS with gentle stirring (100 rpm) at 37 °C. At the desired time points (8, 24, 48, and 72h), 4 mL of dialysate were removed and replaced with 4 mL of fresh PBS. Collected samples were freeze-dried. In order to remove inorganic salts, the dried samples were dissolved in methanol (1 mL), filtered, evaporated, and dried in vacuum. The dried samples containing released BuOE were then reconstituted in water, and BuOE content was determined by comparing the absorbance at 455 nm to a standard curve.

2.6. Electron Paramagnetic Resonance spectroscopy

The ability of BuOE (native and released from nanoBuOE) and nanoBuOE (intact) to scavenge $O_2^{\bullet-}$ was measured via Electron Paramagnetic Resonance (EPR) spectroscopy and the CMH spin probe in a cell free system, as previously described [23,24]. $O_2^{\bullet-}$ was generated with HX and XO. Samples contained 200 μM CMH, 50 μM HX, and 10 mU/mL XO in 200 μL KDD buffer (pH 7.4). KDD buffer was made up of Krebs-HEPES buffer consisting of (in mM): 99 NaCl, 4.69 KCl, 2.5 $CaCl_2$, 1.2 $MgSO_4$, 25 $NaHCO_3$, 1.03 KH_2PO_4, 5.6 D-glucose, and 20 HEPES. The KDD buffer was supplemented with metal chelators DETC (5 μM) and DF (25 μM). Experimental groups included 400 U/mL SOD protein, native BuOE (10–50 nM), intact nanoBuOE (50 nM), and BuOE released from nanoBuOE (50 nM). Samples were incubated for 30 min at 37 °C in a heat block, and 50 μL of sample was loaded into a glass capillary tube before being placed in the capillary holder of the Bruker e-Scan Table-top EPR Spectrometer. The EPR Spectrometer settings were as follows: Field Sweep Width: 60 G, Microwave Frequency: 9.72 GHz, Microwave power: 21.9 mW, Modulation Amplitude: 2.37 G, Conversion Time: 10.24 ms, Time Constant: 40.96 ms.

To test the ability of native BuOE to scavenge H_2O_2, KDD+ buffer was used, which consists of the KDD buffer described above, supplemented with AAP (1 mM), HRP (1 U/mg) and DTPA (200 μM), as previously described [23]. Cell-free samples contained 200 μM CMH and 10 μM H_2O_2 in 200 μL of KDD+ buffer. The different experimental groups included 400 U/mL catalase protein, a H_2O_2 scavenger, and native BuOE (10–100 μM). Samples were incubated as described above, and the EPR spectra were obtained and analyzed for changed in amplitude.

Table 1
Physicochemical characteristics of mesoporous silica nanoparticles.

Nanoparticle Formulation	Coating	D_{eff} (nm)	PDI	ζ-potential (mV)
Empty	None	47 ± 1	0.14	−16 ± 2
BuOE-loaded	Lipid	56 ± 2	0.18	3 ± 1

Particle size (D_{eff}), polydispersity index (PDI) and ζ-potential were determined by DLS (0.5 mg/mL, PBS, pH 7.4, 25 °C). Data presented as mean ± SD (n = 3). BuOE-loaded nanoparticles were stable for at least 2 weeks without aggregation.

2.7. Blood pressure measurements

Male C57Bl/6 mice, 9–10 weeks old, (20–25 g, Jackson Laboratories, Bar Harbor, ME) were housed in the animal facility with a 12 h light-dark cycle. Animals had access to standard chow and water *ad libitum*. Upon arrival to the UNMC animal facility, mice were allowed to acclimate in their home cages for one week. Following the acclimation, mice were implanted with radiotelemeters (PhysioTel PA-C10, Data Sciences International, St. Paul, MN), as previously described [24,25], to record blood pressure. Briefly, mice were anesthetized with isoflurane inhalation (2.5%) and kept under anesthesia by isoflurane inhalation (1–2%) for the duration of the procedure. After isolation of the left carotid artery, the catheter of the telemeter was inserted into the carotid artery. The body of the telemeter was placed in a subcutaneous pouch on the right side of the mouse. The incision was closed with 6.0 Prolene suture (Ethicon) and treated with bupivacaine (1 mg/kg, subcutaneous) immediately following the procedure. Daily recordings in conscious, unrestrained mice monitored mean arterial pressure (MAP), systolic blood pressure (SBP), and diastolic blood pressure (DBP).

Once a consistent baseline blood pressure was achieved for three consecutive days, mice were intraperitoneally (IP) injected with 100 μL of vehicle (saline), BuOE (1 mg/kg), or nanoBuOE (1 mg/kg). Upon completion of the studies, mice were euthanized with an overdose of pentobarbital (150 mg/kg, IP). All procedures were performed in accordance with institutional guidelines for animal research reviewed and approved by the University of Nebraska Medical Center Institutional Animal Care and Use Committee.

2.8. Renal sympathetic nerve recordings

Male Sprague Dawley rats (300–500 g, Charles River Laboratories, Wilmington, MA) were used to record renal sympathetic nerve activity (RSNA). Rats were housed in the animal facility with a 12 h light-dark cycle with access to standard chow and water *ad libitium*. Upon arrival rats were allowed to acclimate for one week before RSNA was recorded, as previously described [26,27]. Briefly, rats were anesthetized with an IP injection of urethane (0.75 g/kg) and α-chloralose (70 mg/kg). The right femoral artery was cannulated with PE-50 polyethylene tubing connected to a pressure transducer (PowerLab Data-Acquistion System, ADInstruments, Colorado Springs, CO) to measure MAP and heart rate (HR). Similarly, the right femoral vein was cannulated to administer the drugs intravenously (IV). After a tracheal intubation to allow for independent breathing, a retroperitoneal flank incision was made to expose the left kidney and to identify the renal artery and vein. Next, a branch of the renal nerve was isolated and placed on a bipolar platinum electrode. The nerve/electrode junction was surrounded with WACKER SilGel mixture (604 & 601) to isolate the junction, thereby reducing the noise to signal ratio and prolonging the duration of a good signal. The electrical signal was amplified via a Grass amplifier with high- and low-frequency cutoffs of 1000 Hz and 100 Hz, respectively. The rectified output (resister capacitor) filtered time constant (0.5 s) was then recorded and integrated using PowerLab (8si, ADInstruments, Sydney, NSW, Australia). After approximately 30 min of stable baseline recording, BuOE or nanoBuOE (0.1 mg/kg, IV) was administered, and changes in MAP, HR, and RSNA were monitored. Following the completion of this protocol, hexamethonium (120 mg/mL, IV) was administered to determine the amount of background noise in the signal. Basal nerve activity was determined at the beginning of the experiment, and background noise was determined by nerve activity recorded at the end of the experiment. The RSNA during the experiment was calculated by subtracting the background noise from the recorded value. The RSNA response to injection of drugs was expressed as a percentage change from the basal value. All procedures were performed in accordance with

institutional guidelines for animal research reviewed and approved by the University of Nebraska Medical Center Institutional Animal Care and Use Committee.

2.9. Statistical analysis

All data are expressed as mean ± standard error of the mean (SEM). One-way ANOVA followed by Bonferroni Post-Hoc test were used to analyze the nanoBuOE release studies and the EPR spectroscopy experiments. For the blood pressure measurements, data were analyzed by two-way ANOVA followed by Bonferroni Post-Hoc test. Treatment indicates a difference between various treatment groups (vehicle, BuOE, and nanoBuOE). Time indicates a difference over time. Interaction indicates whether the effect of treatment depends on the effect of time. For renal sympathetic nerve recordings, the data were analyzed via two-way ANOVA followed by Bonferroni Post-Hoc test. A p-value less than 0.05 was considered to be statistically significant. To estimate effect sizes, partial omega square (ω_p^2) analysis was performed. Statistical analyses were completed using Prism 8 (GraphPad Software, Inc).

3. Results

3.1. Native BuOE scavenges superoxide, but not hydrogen peroxide

To confirm BuOE's ability to scavenge $O_2^{\bullet-}$, a cell-free system utilizing hypoxanthine (HX) and xanthine oxidase (XO) in the presence or absence of BuOE was subject to EPR spectroscopy. These cell-free reactions contained the CMH spin probe, which reacts with $O_2^{\bullet-}$ produced by HX + XO, yielding the spin probe radical ($CM^{\bullet}$) that is detected by the EPR spectrometer. The amplitude of the EPR spectrum is directly proportional to the levels of free radicals in the sample [28]. Native BuOE (25–50 nM) decreased the EPR spectrum amplitude indicating a decrease in $O_2^{\bullet-}$ levels (Fig. 2A and B). CuZnSOD protein (400 U/mL) was used to validate that $O_2^{\bullet-}$ was being measured as addition of CuZnSOD protein virtually abolished the EPR spectrum amplitude.

To determine if BuOE could scavenge H_2O_2, EPR spectroscopy was used to measure the levels of H_2O_2 in cell-free reactions containing H_2O_2 and CMH in the presence or absence of BuOE. Since H_2O_2 reacts very poorly with CMH [29], these reactions were supplemented with AAP and HRP. In the presence of H_2O_2, HRP catalyzes the oxidation of AAP to a phenoxyl radical, which reacts with CMH to form $CM^{\bullet}$. Thus, the more H_2O_2 in the sample, the larger the EPR spectrum amplitude. BuOE (10–100 nM) failed to decrease the EPR spectrum amplitude in the presence of H_2O_2 (Fig. 2C and D). Meanwhile, catalase (400 U/mL) significantly attenuated the EPR spectrum amplitude validating that H_2O_2 was indeed being measured. Together, these results indicate that native BuOE scavenges $O_2^{\bullet-}$ but not H_2O_2.

3.2. BuOE is slowly released from nanoBuOE

The mesoporous silica nanoformulation was selected based on its potential to slowly release the encapsulated drug. To confirm the slow release of BuOE, we performed an *in vitro* release study. BuOE was slowly released from the silica nanoparticles over 72 h (Fig. 3A). The BuOE from the nanoformulation was subject to EPR spectroscopy to confirm the ability of the released drug to scavenge $O_2^{\bullet-}$. Released BuOE significantly decreased the EPR spectrum amplitude, while intact nanoBuOE (nanoBuOE that was not subject to release) did not (Fig. 3B). These results confirm the ability of nanoBuOE to slowly release BuOE over time while maintaining BuOE's SOD-like properties.

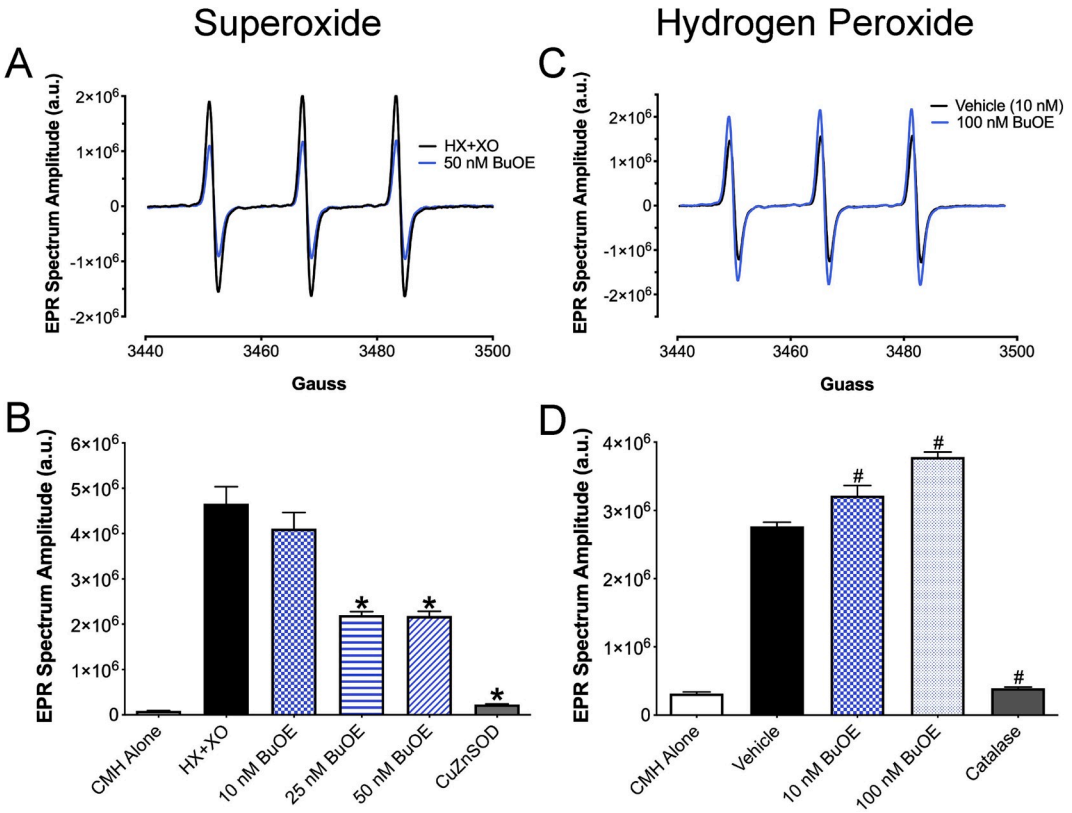

Fig. 2. BuOE scavenges superoxide, but not hydrogen peroxide. A) Representative EPR spectra from cell-free samples containing hypoxanthine (HX) + xanthine oxidase (XO) in the presence or absence of BuOE (50 nM). B) Summary EPR data showing a dose response of BuOE (10–50 nM) in cell-free samples with HX + XO and CMH. CuZnSOD protein: 400 U/mL. *$p < 0.05$ vs HX + XO. n = 4–8. C) Representative EPR spectra from cell-free samples containing H_2O_2 in the presence or absence of BuOE (100 nM) in KDD+ buffer. D) Summary EPR data showing a dose response of BuOE (10–100 nM) in cell-free samples with H_2O_2. Vehicle = H_2O_2 alone. Catalase protein: 400 U/mL. #$p < 0.05$ vs Vehicle. n = 3.

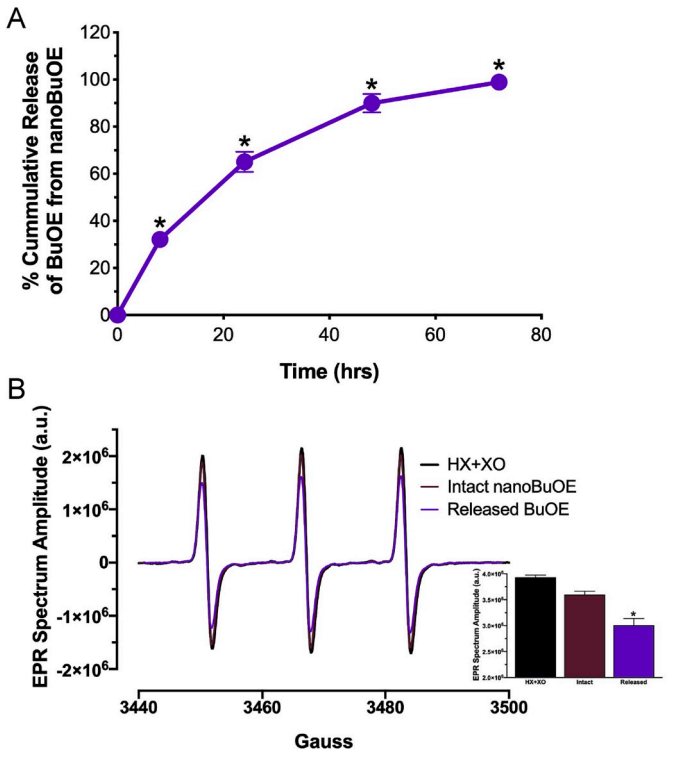

Fig. 3. BuOE is released from its nanoencapsulation over 72 h and remains active. A) After 72 h at 37 °C, 99% of BuOE is released from nanoBuOE. *p < 0.05 vs 0 time point. n = 5. B) Representative EPR spectra from cell-free reactions containing HX + XO and CMH in the presence or absence of BuOE released from nanoBuOE (Released BuOE, 50 nM) or intact nanoBuOE (50 nM). Inset: Summary EPR data showing released BuOE (50 nM) and intact nanoBuOE (50 nM). *p < 0.05 vs HX + XO. n = 4.

3.3. Native BuOE, but not nanoBuOE, acutely decreases blood pressure in mice

To determine if BuOE and nanoBuOE decrease blood pressures in mice, native BuOE (1 mg/kg), nanoBuOE (1 mg/kg) or vehicle (100 μL) was injected IP into mice and blood pressure monitored for 2 h. Native BuOE significantly decreased SBP (Fig. 4A), DBP (Fig. 4B), and MAP (Fig. 4C) immediately following the injection. Meanwhile, nanoBuOE had no effect on SBP, DBP or MAP (Fig. 4). It is important to note that the blood pressures at the time of injection are slightly higher than the typical 95–100 mmHg seen in normotensive mice at baseline. This elevation in blood pressure is due to animal handling for IP injections. The gradual decrease in blood pressure seen in the vehicle- and nanoBuOE-treated animals is a result of the animals acclimating to their home cage post-injection. These data suggest that BuOE encapsulated in mesoporous silica nanoparticles as intact nanoBuOE prevents the immediate and transient decrease in systolic, diastolic, and mean arterial pressures.

3.4. Native BuOE, but not nanoBuOE, transiently decreases renal sympathetic nerve activity (RSNA)

To begin investigating mechanisms involved in the native BuOE-induced hypotensive response, we measured changes in the sympathetic nervous system (SNS), which is known to play an integral role in blood pressure regulation [30,31]. More specifically, we measured RSNA in anesthetized rats injected IV with native BuOE or nanoBuOE (0.1 mg/kg). Ten-second representative RSNA recordings in Fig. 5A show that native BuOE induces an immediate (within 10 s) decrease in RSNA, followed by a steady increase in RSNA thereafter (Fig. 5A and C).

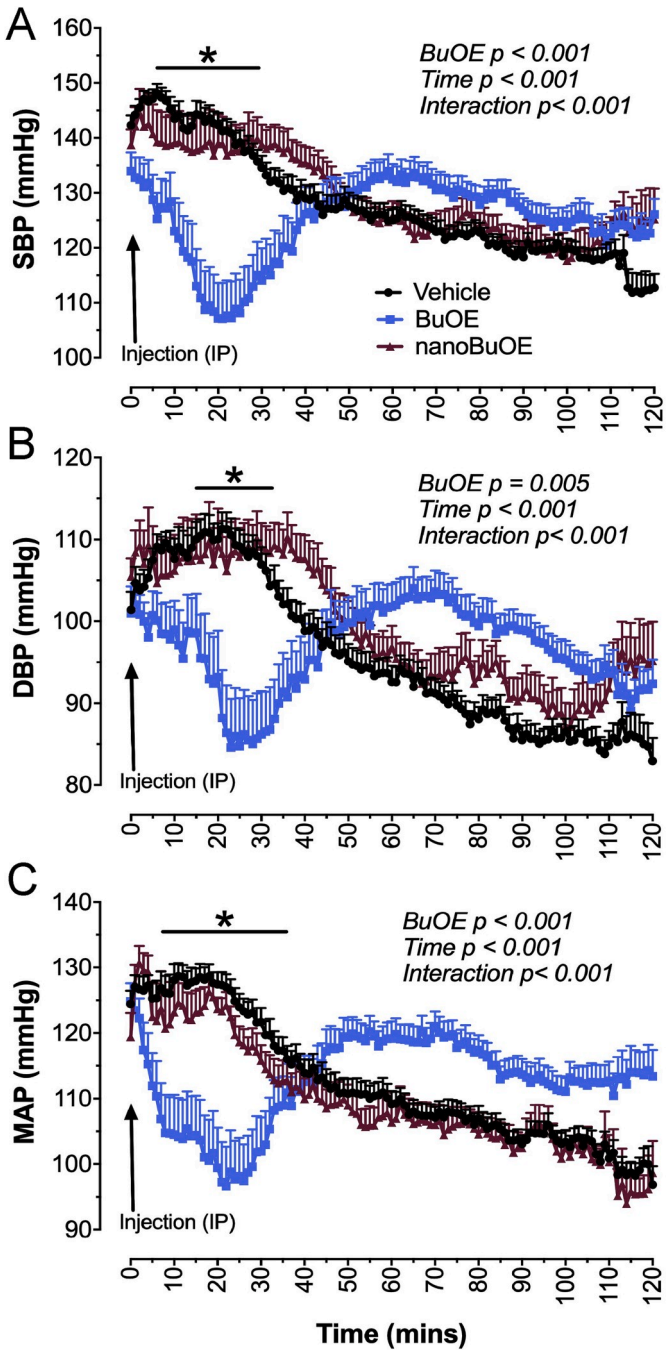

Fig. 4. BuOE, but not nanoBuOE (1 mg/kg, IP), rapidly and acutely decreases blood pressure in mice. A) Summary systolic blood pressure (SBP) data of mice given BuOE, nanoBuOE, or vehicle (saline). B) Summary diastolic blood pressure (DBP) data of mice given BuOE, nanoBuOE or vehicle. C) Summary mean arterial pressure (MAP) data of mice given BuOE, nanoBuOE, or vehicle. *p < 0.05 between BuOE- and vehicle-treated animals. n = 27 (Vehicle), 19 (BuOE), 16 (nanoBuOE). MAP $\omega_p^2 = 0.876$.

This rapid decrease in RSNA occurs with a concomitant decrease in MAP that lasts approximately 30 min after the injection (Fig. 5D). The decrease in RSNA and MAP is followed by an increase in HR (Fig. 5E). In contrast, nanoBuOE-treated rats did not exhibit a decrease in RSNA, had a minimal decrease in MAP, and had no change in HR (Fig. 5B–E). These results suggest that native BuOE, but not nanoBuOE, induces acute hypotension, at least in part, by inhibiting the SNS.

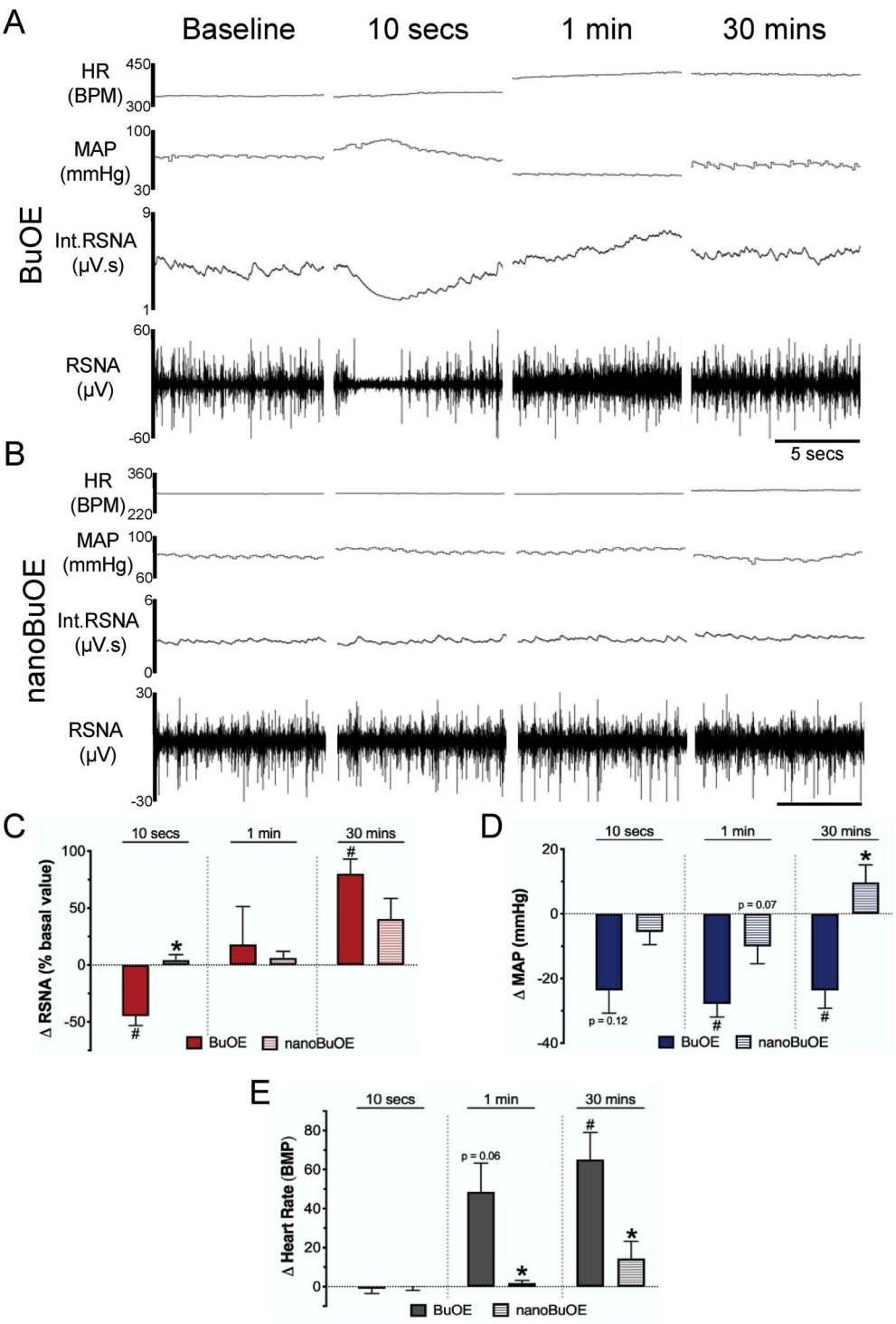

Fig. 5. Native BuOE, but not nanoBuOE (0.1 mg/kg, IV), transiently decreases renal sympathetic nerve activity (RSNA) and blood pressure (BP) in rats. Representative tracings of heart rate (HR), mean arterial pressure (MAP), integrated (Int) RSNA and raw RSNA in A) native BuOE- or B) nanoBuOE-injected rats at baseline, 10 s, 1 min and 30 min. C) Summary data showing change in RSNA as a percent of baseline. RSNA $\omega_p^2 = 0.356$. D) Summary data showing change in MAP from baseline. MAP $\omega_p^2 = 0.813$. $p = 0.12$ vs baseline. $p = 0.07$ vs BuOE. E) Summary data showing change in HR from baseline. HR $\omega_p^2 = 0.684$. $p = 0.06$ vs baseline. *$p < 0.05$ vs BuOE-treated rats. #$p < 0.05$ vs baseline. $n = 6$ (BuOE), 7 (nanoBuOE).

4. Discussion

The role of $O_2^{\bullet-}$ and other ROS in a plethora of pathological conditions such as cancers and cardiovascular diseases has brought about several decades of work on SOD mimics [2]. One major class of SOD mimics are manganese porphyrins such as MnTE-2-PyP^{5+} (T2E) and MnTnBuOE-2-PyP^{5+} (BuOE). BuOE is one of the most recently formulated manganese porphyrin SOD mimics with a manganese metal center surrounded by a porphyrin ring. The manganese metal center contains a positive charge along with four other positive charges on its constituents that help attract $O_2^{\bullet-}$, allowing it to be oxidized and reduced [2]. Previous manganese porphyrin SOD mimics, such as T2E, have limited biodistribution and cannot cross the blood brain barrier [32,33]. To facilitate increased biodistribution of BuOE, alkyl chains were lengthened which increased lipophilicity. Additionally, oxygen was added within the lengthy alkyl chains to reduce toxicity. The enhanced biodistribution and limited toxicity [14,33] has advanced BuOE and its therapeutic benefits into numerous clinical trials as a radioprotector for cancer patients (BMX-001 ClinicalTrials.gov Identifiers: NCT02655601, NCT02990468, NCT03386500, NCT03608020). However, an adverse side effect of high dose BuOE, as reported in non-human primates and dogs, is dysregulation of cardiovascular homeostasis including an acute

and robust decrease in arterial blood pressure and an increase in heart rate [16]. In the present study, we investigated the impact of a mesoporous silica nanoformulation of BuOE, so-called nanoBuOE, which slowly releases active BuOE, on cardiovascular function. We report that BuOE, but not nanoBuOE, causes an acute and significant decrease in arterial blood pressure that is concurrent with inhibition of the sympathetic nervous system. This study demonstrates that nanoBuOE protects against the immediate and acute decrease in arterial blood pressure as well as the transient decrease of sympathetic nerve activity due to the slow and sustained release of BuOE from the nanoformulation.

Numerous formulations of nanomaterials exist and have been utilized in a variety of cardiovascular and oxidative stress studies, each with their own strengths and weaknesses [18]. Our nanoBuOE is structured with BuOE encapsulated in mesoporous silica nanoparticles. These particles are known to offer a slow, sustained release and are used in a variety of sustained drug delivery systems [17,18]. The silica nanoparticles embedded with BuOE are further wrapped in a lipid bilayer to help increase the lipophilicity of the molecule. The resulting lipid-coated mesoporous silica nanoparticles have been shown to improve the efficacy and safety of irinotecan delivery [21], as well as the synergistic delivery of gemcitabine and paclitaxel in mice with pancreatic cancer [20]. The present study demonstrates the lipid-coated mesoporous silica nanoparticles that encapsulate BuOE slowly release the drug over the course of 72 h. Importantly, upon release from the nanoformulation, BuOE retains its ability to scavenge $O_2^{\bullet-}$ and does so to a similar extent as native BuOE. In contrast, intact nanoBuOE lacks SOD activity as evidenced by no significant decrease in the EPR spectrum amplitude obtained from samples containing the intact nanoformulation. We speculate that this lack of SOD activity is due to the lipid bilayer of the nanoparticle preventing $O_2^{\bullet-}$ from accessing the BuOE active site.

Our data demonstrate that native BuOE and BuOE released from nanoBuOE scavenge $O_2^{\bullet-}$ but not H_2O_2 as measured by EPR spectroscopy. These data are in agreement with many studies using manganese porphyrin SOD mimics conducted over the last several decades [2,14,34,35]. Furthermore, the inability of BuOE to scavenge H_2O_2 is in agreement with previous work suggesting that BuOE has such minimal catalase-like activity that it is not biologically relevant [36]. In addition, our data support numerous observations that manganese porphyrins promote altered cell signaling and cell death in cancer cells through the accumulation of H_2O_2 to toxic levels [4,37,38].

Based on the established role of $O_2^{\bullet-}$ in cardiovascular pathologies such as hypertension [1,39], BuOE's ability to scavenge $O_2^{\bullet-}$, and BuOE's impact on cardiovascular function as reported in non-clinical safety and toxicology studies [16], we sought to determine BuOE's and nanoBuOE's effect on blood pressure in conscious mice. Our results show that a single IP bolus injection of BuOE, but not nanoBuOE, significantly decreases systolic, diastolic, and mean arterial pressure beginning immediately after injection with the peak hypotensive response approximately 20–25 min post-injection. We observed a similar response in anesthetized rats. This BuOE-induced hypotensive response is consistent with a decrease in blood pressure observed in dogs [16]. In a phase I clinical trial, cancer patients receiving the highest dose of BuOE as a radioprotector also displayed a decrease in blood pressure (unpublished findings). BuOE at three lower doses did not elicit this hypotensive response, and these lower doses appear to be efficacious in preventing radiation damage. However, in patients with dysregulated blood pressure or cardiovascular complications, having a way to mitigate this potential adverse side effect may prove beneficial.

Our results are also in agreement with hemodynamic data collected from anesthetized rats treated with the manganese porphyrin, T2E. Ross et al., reported that T2E decreases arterial blood pressure in anesthetized rats at a dose of 5 μg/kg (IV) [40], which resembles our results in anesthetized rats treated with BuOE (0.1 mg/kg, IV). However, the same study did not report a significant decrease in arterial blood pressure in anesthetized mice treated with T2E (100-2000 μg/kg, IV) [40]; whereas, our results show that 1 mg/kg BuOE (IP) dramatically decreases arterial blood pressure in conscious mice immediately after injection. The discrepancies in responses between these studies may be attributed to the differences in: 1) SOD mimics (T2E vs BuOE); 2) route of administration (IV vs IP); or, 3) state of animal consciousness (anesthetized vs conscious).

To begin exploring the mechanism by which BuOE acutely decreases arterial blood pressure, we measured changes in RSNA to evaluate the contribution of the sympathetic nervous system. By directly influencing cardiac, vascular, renal, and immune cell function, the sympathetic nervous system is known to play a key role in overall blood pressure regulation both acutely as well as chronically [30,31]. Furthermore, numerous studies have clearly described the contribution of elevated sympathetic nerve activity to pathophysiological conditions such as hypertension and heart failure [31,41]. In our studies described here, we directly recorded RSNA in anesthetized rats. It should be noted that the dose used for these anesthetized rat studies (0.1 mg/kg) was ten times less than that given IP to mice (1 mg/kg) in our acute blood pressure studies. The dose for rats was determined based on our preliminary observations that rats were more sensitive to the drug, especially following an IV injection. Immediately (within 10 s) following injection of BuOE, but not nanoBuOE, RSNA decreased significantly compared to baseline. Although the underlying mechanism(s) by which BuOE induces this acute sympathoinhibition requires additional investigation, we speculate that BuOE, which can cross the blood-brain barrier [6,7,33], scavenges $O_2^{\bullet-}$ in brain nuclei known to control cardiovascular function by mediating sympathetic drive. In fact, it has been reported numerous times by us and others that scavenging $O_2^{\bullet-}$ in these unique brain regions decreases elevated arterial blood pressure [23,24,42–46]. Interestingly, we observed that following the BuOE-induced acute sympathoinhibition, RSNA underwent a gradual and prolonged increase, surpassing baseline levels. This sympathoexcitation is likely a baroreflex-mediated compensatory attempt to restore arterial blood pressure back to normal levels. The significant increase in HR compared to baseline we observed is also indicative of an increase in sympathetic nerve activity to the heart and is in agreement with BuOE's non-clinical safety and toxicology studies performed in non-human primates [16].

Arterial blood pressure regulation is not only influenced by the sympathetic nervous system, but also by many peripheral mechanisms and organs including the vasculature [39]. The BuOE-induced decrease in arterial blood pressure reported herein may be the result of BuOE scavenging $O_2^{\bullet-}$ in the vasculature, which would likely lead to increase nitric oxide ($^{\bullet}NO$) bioavailability. Considering $^{\bullet}NO$ is also a well-known vasodilator, elevated levels of $^{\bullet}NO$ in the vasculature would result in vasodilation and a subsequent decrease in arterial blood pressure. Studies are currently underway in our laboratory to address this hypothesis.

In conscious mice, IP-injected nanoBuOE failed to induce an immediate decrease in arterial blood pressure, while in anesthetized rats, IV-injected nanoBuOE resulted in a modest, non-significant decrease in arterial blood pressure. The decrease in blood pressure between BuOE- and nanoBuOE-treated rats trends toward significance at 1 min and is significantly different at 30 min post-injection. The differences in arterial blood pressure responses between mice and rats observed in our study are likely due to the increased sensitivity of rats to SOD mimics compared to other species [40]. NanoBuOE-treated rats had no change in RSNA at the immediate time point, which was significantly different from BuOE-treated rats that experienced an approximate 50% decrease in RSNA. Additionally, there was little change in HR in nanoBuOE-treated rats, which is significantly different from the increase in HR observed in BuOE-treated animals.

The primary limitation with the current study is the lack of understanding the biodistribution of nanoBuOE. While numerous studies have investigated the biodistribution of BuOE in the brain and other organs [2,16,33], it remains unknown whether nanoBuOE follows the same biodistribution pattern as native BuOE. It is possible that, unlike BuOE,

nanoBuOE does not cross the blood brain barrier or is not taken up by the vasculature. Thus, the lack of sympathoinhibition and hypotensive response following nanoBuOE administration may be the result of limited biodistribution of nanoBuOE. Our laboratory is currently conducting biodistribution studies to address this limitation.

5. Conclusion

The present study demonstrates that nanoBuOE protects against the BuOE-induced decrease in arterial blood pressure and prevents the immediate precipitous drop in RSNA. Possible explanations for nanoBuOE's protective effects include the slow release of the drug over time or inactivate BuOE in the nanoformulation. However, our *in vitro* results show that BuOE released from nanoBuOE retains its SOD-like properties suggesting that nanoBuOE's slow and sustained release of the drug prevents the immediate and acute effects of native BuOE. Further characterization and exploration of nanoBuOE's therapeutic effects may not only improve the safety profile of BuOE as a radioprotector in cancer patients, but may also be a viable option as a novel anti-hypertensive therapeutic.

Declaration of competing interest

The authors declare the following financial interests/personal relationships which may be considered as potential competing interests: Dr. Oberley-Deegan is a consultant with BioMimetix Pharmaceutical, Inc. and holds equities in BioMimetix Pharmaceutical, Inc. There are no other conflicts of interest reported by the authors.

Acknowledgements

This project was supported, in part, by the UNMC Center for Heart and Vascular Research (CHVR), and by the National Institute of General Medical Sciences, 1U54GM115458, which funds the Great Plains IDeA-CTR Network. This work was also supported by the National Institutes of Health grants R01DK114663 and P01HL62222 (to K.P. Patel), as well as R01CA178888 and SP20GM103480 (to R.E. Oberley-Deegan), and an endowed McIntyre Professorship to K.P. Patel. The content is solely the responsibility of the authors and does not necessarily represent the official views of CHVR or the NIH. EPR spectroscopy data was collected in the University of Nebraska's EPR Spectroscopy Core, which was initially established with support from a Center of Biomedical Research Excellence grant from the National Institute of General Medical Sciences of the National Institutes of Health (P30GM103335) awarded to the University of Nebraska's Redox Biology Center. We also acknowledge the assistance of the Nanomaterials Core Facility of the Center for Biomedical Research Excellence, Nebraska Center for Nanomedicine supported by the Institutional Development Award from the National Institute of General Medical Sciences of the National Institutes of Health under grant number P30GM127200.

References

[1] D.I. Brown, K.K. Griendling, Regulation of signal transduction by reactive oxygen species in the cardiovascular system, Circ. Res. 116 (2015) 531–549, https://doi.org/10.1161/CIRCRESAHA.116.303584.

[2] I. Batinic-Haberle, A. Tovmasyan, I. Spasojevic, Mn porphyrin-based redox-active drugs: differential effects as cancer therapeutics and protectors of normal tissue against oxidative injury, Antioxidants Redox Signal. 29 (2018) 1691–1724, https://doi.org/10.1089/ars.2017.7453.

[3] I. Batinic-Haberle, A. Tovmasyan, I. Spasojevic, An educational overview of the chemistry, biochemistry and therapeutic aspects of Mn porphyrins – from superoxide dismutation to H2O2-driven pathways, Redox Biol. 5 (2015) 43–65, https://doi.org/10.1016/j.redox.2015.01.017.

[4] A. Chatterjee, Y. Zhu, Q. Tong, E. Kosmacek, E. Lichter, R. Oberley-Deegan, The addition of manganese porphyrins during radiation inhibits prostate cancer growth and simultaneously protects normal prostate tissue from radiation damage, Antioxidants 7 (2018) 21, https://doi.org/10.3390/antiox7010021.

[5] S. Shrishrimal, E. Kosmacek, A. Chatterjee, M. Tyson, R. Oberley-Deegan, The SOD mimic, MnTE-2-PyP, protects from chronic fibrosis and inflammation in irradiated normal pelvic tissues, Antioxidants 6 (2017) 87, https://doi.org/10.3390/antiox6040087.

[6] D.H. Weitzel, A. Tovmasyan, K.A. Ashcraft, Z. Rajic, T. Weitner, C. Liu, W. Li, A. F. Buckley, M.R. Prasad, K.H. Young, R.M. Rodriguiz, W.C. Wetsel, K.B. Peters, I. Spasojevic, J.E. Herndon, I. Batinic-Haberle, M.W. Dewhirst, Radioprotection of the brain white matter by Mn(III) N-Butoxyethylpyridylporphyrin-Based superoxide dismutase mimic MnTnBuOE-2-PyP5+, Mol. Canc. Therapeut. 14 (2015) 70–79, https://doi.org/10.1158/1535-7163.MCT-14-0343.

[7] D.H. Weitzel, A. Tovmasyan, K.A. Ashcraft, A. Boico, S.R. Birer, K. Roy Choudhury, J. Herndon, R.M. Rodriguiz, W.C. Wetsel, K.B. Peters, I. Spasojevic, I. Batinic-Haberle, M.W. Dewhirst, Neurobehavioral radiation mitigation to standard brain cancer therapy regimens by Mn(III) *n* -butoxyethylpyridylporphyrin-based redox modifier: brain Radiation Mitigation by MnTnBuOE-2-PyP $^{5+}$, Environ. Mol. Mutagen. 57 (2016) 372–381, https://doi.org/10.1002/em.22021.

[8] K.A. Ashcraft, M.-K. Boss, A. Tovmasyan, K. Roy Choudhury, A.N. Fontanella, K. H. Young, G.M. Palmer, S.R. Birer, C.D. Landon, W. Park, S.K. Das, T. Weitner, H. Sheng, D.S. Warner, D.M. Brizel, I. Spasojevic, I. Batinic-Haberle, M. W. Dewhirst, Novel manganese-porphyrin superoxide dismutase-mimetic widens the therapeutic margin in a preclinical head and neck cancer model, Int. J. Radiat. Oncol. Biol. Phys. 93 (2015) 892–900, https://doi.org/10.1016/j.ijrobp.2015.07.2283.

[9] S.R. Birer, C.-T. Lee, K.R. Choudhury, K.H. Young, I. Spasojevic, I. Batinic-Haberle, J.D. Crapo, M.W. Dewhirst, K.A. Ashcraft, Inhibition of the continuum of radiation-induced normal tissue injury by a redox-active Mn porphyrin, Radiat. Res. 188 (2017) 94, https://doi.org/10.1667/RR14757.1.S1.

[10] A. Patel, E.A. Kosmacek, K.W. Fisher, W. Goldner, R.E. Oberley-Deegan, MnTnBuOE-2-PyP treatment protects from radioactive iodine (I-131) treatment-related side effects in thyroid cancer, Radiat. Environ. Biophys. 59 (2020) 99–109, https://doi.org/10.1007/s00411-019-00820-2.

[11] H. Li, Y. Wang, S.K. Pazhanisamy, L. Shao, I. Batinic-Haberle, A. Meng, D. Zhou, Mn(III) meso-tetrakis-(N-ethylpyridinium-2-yl) porphyrin mitigates total body irradiation-induced long-term bone marrow suppression, Free Radic. Biol. Med. 51 (2011) 30–37, https://doi.org/10.1016/j.freeradbiomed.2011.04.016.

[12] B. Gauter-Fleckenstein, K. Fleckenstein, K. Owzar, C. Jiang, I. Batinic-Haberle, Z. Vujaskovic, Comparison of two Mn porphyrin-based mimics of superoxide dismutase in pulmonary radioprotection, Free Radic. Biol. Med. 44 (2008) 982–989, https://doi.org/10.1016/j.freeradbiomed.2007.10.058.

[13] B. Gauter-Fleckenstein, K. Fleckenstein, K. Owzar, C. Jiang, J.S. Rebouças, I. Batinic-Haberle, Z. Vujaskovic, Early and late administration of MnTE-2-PyP5+ in mitigation and treatment of radiation-induced lung damage, Free Radic. Biol. Med. 48 (2010) 1034–1043, https://doi.org/10.1016/j.freeradbiomed.2010.01.020.

[14] Z. Rajic, A. Tovmasyan, I. Spasojevic, H. Sheng, M. Lu, A.M. Li, E.B. Gralla, D. S. Warner, L. Benov, I. Batinic-Haberle, A new SOD mimic, Mn(III) ortho N-butoxyethylpyridylporphyrin, combines superb potency and lipophilicity with low toxicity, Free Radic. Biol. Med. 52 (2012) 1828–1834, https://doi.org/10.1016/j.freeradbiomed.2012.02.006.

[15] Search of, BMX-001 - list results - ClinicalTrials.gov (n.d.), https://clinicaltrials.gov/ct2/results?cond=&term=BMX-001&cntry=&state=&city=&dist=. accessed April 20, 2020).

[16] S.C. Gad, D.W. Sullivan, I. Spasojevic, C.V. Mujer, C.B. Spainhour, J.D. Crapo, Nonclinical safety and toxicokinetics of MnTnBuOE-2-PyP $^{5+}$ (BMX-001), Int. J. Toxicol. 35 (2016) 438–453, https://doi.org/10.1177/1091581816642766.

[17] F. Tang, L. Li, D. Chen, Mesoporous silica nanoparticles: synthesis, biocompatibility and drug delivery, Adv. Mater. 24 (2012) 1504–1534, https://doi.org/10.1002/adma.201104763.

[18] Y. Wang, Q. Zhao, N. Han, L. Bai, J. Li, J. Liu, E. Che, L. Hu, Q. Zhang, T. Jiang, S. Wang, Mesoporous silica nanoparticles in drug delivery and biomedical applications, Nanomed. Nanotechnol. Biol. Med. 11 (2015) 313–327, https://doi.org/10.1016/j.nano.2014.09.014.

[19] H. Yamada, C. Urata, H. Ujiie, Y. Yamauchi, K. Kuroda, Preparation of aqueous colloidal mesostructured and mesoporous silica nanoparticles with controlled particle size in a very wide range from 20 nm to 700 nm, Nanoscale 5 (2013) 6145, https://doi.org/10.1039/c3nr00334e.

[20] H. Meng, M. Wang, H. Liu, X. Liu, A. Situ, B. Wu, Z. Ji, C.H. Chang, A.E. Nel, Use of a lipid-coated mesoporous silica nanoparticle platform for synergistic gemcitabine and paclitaxel delivery to human pancreatic cancer in mice, ACS Nano 9 (2015) 3540–3557, https://doi.org/10.1021/acsnano.5b00510.

[21] X. Liu, A. Situ, Y. Kang, K.R. Villabroza, Y. Liao, C.H. Chang, T. Donahue, A.E. Nel, H. Meng, Irinotecan delivery by lipid-coated mesoporous silica nanoparticles shows improved efficacy and safety over liposomes for pancreatic cancer, ACS Nano 10 (2016) 2702–2715, https://doi.org/10.1021/acsnano.5b07781.

[22] S. D'Souza, A review of *in vitro* drug release test methods for nano-sized dosage forms, Adv. Pharma. (2014) 1–12, https://doi.org/10.1155/2014/304757, 2014.

[23] E.G. Rosenbaugh, J.W. Roat, L. Gao, R.-F. Yang, D.S. Manickam, J.-X. Yin, H. D. Schultz, T.K. Bronich, E.V. Batrakova, A.V. Kabanov, I.H. Zucker, M. C. Zimmerman, The attenuation of central angiotensin II-dependent pressor response and intra-neuronal signaling by intracarotid injection of nanoformulated copper/zinc superoxide dismutase, Biomaterials 31 (2010) 5218–5226, https://doi.org/10.1016/j.biomaterials.2010.03.026.

[24] K. Savalia, D.S. Manickam, E.G. Rosenbaugh, J. Tian, I.M. Ahmad, A.V. Kabanov, M.C. Zimmerman, Neuronal uptake of nanoformulated superoxide dismutase and attenuation of angiotensin II-dependent hypertension after central administration, Free Radic. Biol. Med. 73 (2014) 299–307, https://doi.org/10.1016/j.freeradbiomed.2014.06.001.

[25] U. Basu, A.J. Case, J. Liu, J. Tian, Y.-L. Li, M.C. Zimmerman, Redox-sensitive calcium/calmodulin-dependent protein kinase IIα in angiotensin II intra-neuronal signaling and hypertension, Redox Biol. 27 (2019) 101230, https://doi.org/10.1016/j.redox.2019.101230.
[26] H. Zheng, X. Liu, Y. Li, K.P. Patel, A hypothalamic leptin-glutamate interaction in the regulation of sympathetic nerve activity, Neural Plast. (2017) 1–11, https://doi.org/10.1155/2017/2361675, 2017.
[27] N.M. Sharma, A.S. Haibara, K. Katsurada, X. Liu, K.P. Patel, Central angiotensin II-Protein inhibitor of neuronal nitric oxide synthase (PIN) axis contribute to neurogenic hypertension, Nitric Oxide 94 (2020) 54–62, https://doi.org/10.1016/j.niox.2019.10.007.
[28] S. Dikalov, K.K. Griendling, D.G. Harrison, Measurement of reactive oxygen species in cardiovascular studies, Hypertension 49 (2007) 717–727, https://doi.org/10.1161/01.HYP.0000258594.87211.6b.
[29] S.I. Dikalov, D.G. Harrison, Methods for detection of mitochondrial and cellular reactive oxygen species, Antioxidants Redox Signal. 20 (2014) 372–382, https://doi.org/10.1089/ars.2012.4886.
[30] N. Charkoudian, J.A. Rabbitts, Sympathetic neural mechanisms in human cardiovascular Health and disease, Mayo Clin. Proc. 84 (2009) 822–830, https://doi.org/10.4065/84.9.822.
[31] J.P. Fisher, J.F.R. Paton, The sympathetic nervous system and blood pressure in humans: implications for hypertension, J. Hum. Hypertens. 26 (2012) 463–475, https://doi.org/10.1038/jhh.2011.66.
[32] T. Weitner, I. Kos, H. Sheng, A. Tovmasyan, J.S. Reboucas, P. Fan, D.S. Warner, Z. Vujaskovic, I. Batinic-Haberle, I. Spasojevic, Comprehensive pharmacokinetic studies and oral bioavailability of two Mn porphyrin-based SOD mimics, MnTE-2-PyP5+ and MnTnHex-2-PyP5+, Free Radic. Biol. Med. 58 (2013) 73–80, https://doi.org/10.1016/j.freeradbiomed.2013.01.006.
[33] D. Leu, I. Spasojevic, H. Nguyen, B. Deng, A. Tovmasyan, T. Weitner, R.S. Sampaio, I. Batinic-Haberle, T.-T. Huang, CNS bioavailability and radiation protection of normal hippocampal neurogenesis by a lipophilic Mn porphyrin-based superoxide dismutase mimic, MnTnBuOE-2-PyP5+, Redox Biol. 12 (2017) 864–871, https://doi.org/10.1016/j.redox.2017.04.027.
[34] A. Chatterjee, E.A. Kosmacek, R.E. Oberley-Deegan, MnTE-2-PyP treatment, or NOX4 inhibition, protects against radiation-induced damage in mouse primary prostate fibroblasts by inhibiting the TGF-beta 1 signaling pathway, Radiat. Res. 187 (2017) 367, https://doi.org/10.1667/RR14623.1.
[35] S.K. Dhar, I. Batinic-Haberle, D.K.S.T. Clair, UVB-induced inactivation of manganese-containing superoxide dismutase promotes mitophagy via ROS-mediated mTORC2 pathway activation, J. Biol. Chem. 294 (2019) 6831–6842, https://doi.org/10.1074/jbc.RA118.006595.
[36] A. Tovmasyan, C.G.C. Maia, T. Weitner, S. Carballal, R.S. Sampaio, D. Lieb, R. Ghazaryan, I. Ivanovic-Burmazovic, G. Ferrer-Sueta, R. Radi, J.S. Reboucas, I. Spasojevic, L. Benov, I. Batinic-Haberle, A comprehensive evaluation of catalase-like activity of different classes of redox-active therapeutics, Free Radic. Biol. Med. 86 (2015) 308–321, https://doi.org/10.1016/j.freeradbiomed.2015.05.018.
[37] E.A. Kosmacek, A. Chatterjee, Q. Tong, C. Lin, R.E. Oberley-Deegan, MnTnBuOE-2-PyP protects normal colorectal fibroblasts from radiation damage and simultaneously enhances radio/chemotherapeutic killing of colorectal cancer cells, Oncotarget 7 (2016), https://doi.org/10.18632/oncotarget.8923.
[38] Q. Tong, Y. Zhu, J.W. Galaske, E.A. Kosmacek, A. Chatterjee, B.C. Dickinson, R. E. Oberley-Deegan, MnTE-2-PyP modulates thiol oxidation in a hydrogen peroxide-mediated manner in a human prostate cancer cell, Free Radic. Biol. Med. 101 (2016) 32–43, https://doi.org/10.1016/j.freeradbiomed.2016.09.019.
[39] R. Loperena, D.G. Harrison, Oxidative stress and hypertensive diseases, Med. Clin. 101 (2017) 169–193, https://doi.org/10.1016/j.mcna.2016.08.004.
[40] A.D. Ross, H. Sheng, D.S. Warner, C.A. Piantadosi, I. Batinic-Haberle, B.J. Day, J. D. Crapo, Hemodynamic effects of metalloporphyrin catalytic antioxidants: structure-activity relationships and species specificity, Free Radic. Biol. Med. 33 (2002) 1657–1669, https://doi.org/10.1016/S0891-5849(02)01140-1.
[41] C.J. Barrett, Renal sympathetic nerves - what have they got to do with cardiovascular disease?: renal sympathetic nerves and cardiovascular disease, Exp. Physiol. 100 (2015) 359–365, https://doi.org/10.1113/expphysiol.2014.080176.
[42] M.C. Zimmerman, E. Lazartigues, J.A. Lang, P. Sinnayah, I.M. Ahmad, D.R. Spitz, R.L. Davisson, Superoxide mediates the actions of angiotensin II in the central nervous system, Circ. Res. 91 (2002) 1038–1045, https://doi.org/10.1161/01.RES.0000043501.47934.FA.
[43] M.C. Zimmerman, E. Lazartigues, R.V. Sharma, R.L. Davisson, Hypertension caused by angiotensin II infusion involves increased superoxide production in the central nervous system, Circ. Res. 95 (2004) 210–216, https://doi.org/10.1161/01.RES.0000135483.12297.e4.
[44] M.-H. Tai, L.-L. Wang, K.L.H. Wu, J.Y.H. Chan, Increased superoxide anion in rostral ventrolateral medulla contributes to hypertension in spontaneously hypertensive rats via interactions with nitric oxide, Free Radic. Biol. Med. 38 (2005) 450–462, https://doi.org/10.1016/j.freeradbiomed.2004.11.015.
[45] J. Collister, M. Bellrichard, D. Drebes, D. Nahey, J. Tian, M. Zimmerman, Over-expression of copper/zinc superoxide dismutase in the median preoptic nucleus attenuates chronic angiotensin II-induced hypertension in the rat, Int. J. Math. Stat. 15 (2014) 22203–22213, https://doi.org/10.3390/ijms151222203.
[46] J.P. Collister, H. Taylor-Smith, D. Drebes, D. Nahey, J. Tian, M.C. Zimmerman, Angiotensin II-induced hypertension is attenuated by overexpressing copper/zinc superoxide dismutase in the brain organum vasculosum of the lamina terminalis, oxidative medicine and cellular longevity, 2016, pp. 1–9, https://doi.org/10.1155/2016/3959087, 2016.